Macromolecules

Article

pubs.acs.org/Macromolecules

Quantitative Imaging of T_g in Block Copolymers by Low-Angle Annular Dark-Field Scanning Transmission Electron Microscopy

Ryotaro Aso,[†,*] Hiroki Kurata,[†] Takeshi Namikoshi,[‡] Tamotsu Hashimoto,[§] Shiao-Wei Kuo,[⊥] Feng-Chih Chang,[⊥] Hirokazu Hasegawa,[∥] Masahiko Tsujimoto,[○] Mikio Takano,[○] and Seiji Isoda[○,*]

[†]Institute for Chemical Research, Kyoto University, Uji 611-0011, Japan

[‡]Kitami Institute of Technology, Kitami, Hokkaido 090-8507, Japan

[§]Graduate School of Engineering, University of Fukui, Fukui 910-8507, Japan

[⊥]Department of Materials and Optoelectronic Science, National Sun Yat-Sen University, Kaohsiung 80424, Taiwan

[∥]Research Administration Center, Graduate School of Engineering, Kyoto University, Kyoto 615-8245, Japan

[○]Institute for Integrated Cell-Material Sciences, Kyoto University, Kyoto 606-8501, Japan

Supporting Information

ABSTRACT: It is often difficult to observe nanoscale structures of polymeric materials using conventional transmission electron microscopy (TEM) because of their weak scattering contrast. To produce quantitative image contrast without any staining, low-angle annular dark-field scanning transmission electron microscopy (LAADF-STEM) was studied for its applicability for observing fine structures in block copolymers. The LAADF-STEM images displayed microphase-separated morphologies of block copolymers with high S/N contrast depending on the intrinsic density difference because of nonstaining. We found that the temperature dependence of the image contrast showed a kink around the glass-transition of the constituent phase, from which one can estimate glass transition temperatures and thermal expansion coefficients at nanoscale. This indicates that the LAADF-STEM imaging is an effective tool to quantitatively image nanoscale phases of polymers.

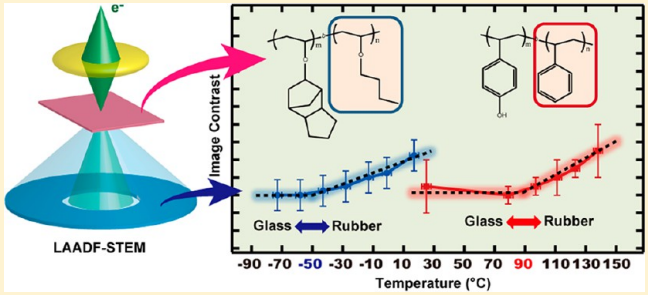

INTRODUCTION

Organic materials represent an important family of materials that exhibit many useful nanoscale functionalities for applications in organic electronics and photonics including organic light-emitting diodes, polymer solar cells, organic thin film transistors, and biofunctional materials.[1−3] In order to understand the structural origins of these functionalities, transmission electron microscopy (TEM) is a powerful tool that provides fundamental structural aspects at the nanoscale. However, it is often difficult to directly observe the fine structures of organic materials using TEM owing to their weak scattering contrast caused by the constituent light elements. In order to form and/or improve the TEM contrast, many technical approaches such as deep defocusing, heavy atom staining (OsO_4 and RuO_4), chemical and physical etching,[4] elemental mapping by electron energy-loss spectroscopy,[5,6] and Zernike phase contrast[7,8] have been applied. Although those methods are highly effective to create contrast, they influence and in some cases modify the intrinsic structure in specimens, and more importantly make it difficult to extract any quantitative image information. Staining, for instance, leads to artifacts caused by swelling of the stained phase and correlated compression of the unstained phase.[9]

Annular dark-field scanning transmission electron microscopy (ADF-STEM) has been used for various atomic analytical applications (Figure S1, Supporting Information).[10,11] ADF-STEM, especially high-angle annular dark-field (HAADF)-STEM, exhibits excellent features for high-resolution observations. HAADF-STEM imaging provides incoherent images attributable in principle to the atomic numbers of the constituent elements (Z-contrast), because the imaging mainly originates from thermal diffuse scattering (TDS) electrons at a high detection angular range, typically higher than 50 mrad. For polymers, there have been many studies so far on HAADF-STEM imaging, including conventional projection 2D imaging as well as tomographic 3D imaging.[12−22] These previous studies focused primarily on the contrast formation itself, even though HAADF-STEM more importantly has the ability to provide quantitative structural information. The image contrast of incoherent HAADF-STEM depends sensitively on local variations in mass thickness difference and density deviation in actual specimens. Therefore, the next challenge is

Received: July 16, 2013
Revised: October 11, 2013
Published: October 29, 2013

   dx.doi.org/10.1021/ma4014934 | Macromolecules 2013, 46, 8589−8595

quantitative analysis of polymers taking advantage of the incoherency in HAADF-STEM.

Low-angle annular dark-field (LAADF)-STEM has been proposed as a suitable alternative imaging technique for radiation-sensitive materials consisting of light elements,[23,24] since LAADF-STEM can utilize more TDS electrons for imaging than HAADF-STEM, as will be described later. LAADF-STEM is commonly known to be useful to visualize strain fields, which can be understood simply as strain being interpreted in terms of the Debye−Waller factor in TDS.[25] In addition to this advantage, it was concluded that the LAADF-STEM image provides almost quantitative *Z*-contrast as does HAADF-STEM, as a result of the very small contribution from Bragg diffraction in organic crystalline films, which was also verified from image simulations. This should also be likely in amorphous materials as copolymers. Recently, Egerton has demonstrated, using simulation, a 10% density change in an amorphous aliphatic material, for which the dose-limited resolution in ADF-STEM shows a broad minimum as a function of the detector angle, wherein the optimum ADF inner angle depends on the specimen thickness and incident electron energy but lies within the range of 10−50 mrad (LAADF condition).[26] In practical terms, LAADF-STEM often gives higher contrast than bright-field (BF) imaging such as BF-STEM and conventional TEM (Figure 1). LAADF-STEM is thus useful not only for strain visualization but also for quantitative high-resolution imaging of radiation-sensitive materials.

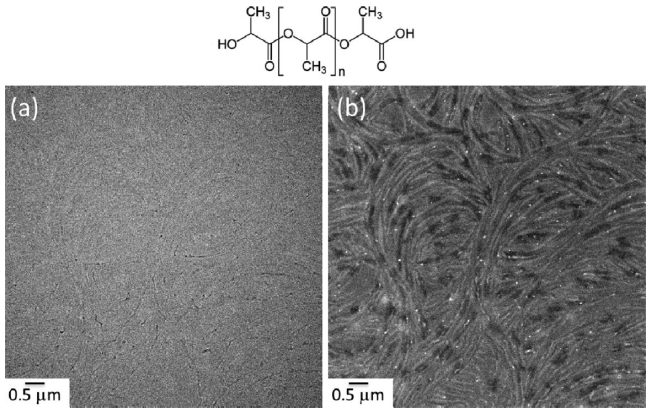

Figure 1. Example of LAADF-STEM observations. (a) Bright-field (BF)-STEM and (b) LAADF-STEM images of a thin crystalline film of polylactide (PLLA). Only faint low contrast is observed in part a, while in part b, curved leaf-vein-like structures are clearly observed with higher contrast. The small bright dots in part b are contamination.

In the present study, we examined the suitability of LAADF-STEM for structure analysis of radiation-sensitive polymer materials and its quantitative application for nanoscale analysis of thermal behavior of block copolymers. We revealed that the LAADF-STEM imaging formed contrast of fine structures in block copolymers without staining. We also successfully detected changes in image intensity for glass-transitions in individual microphase separated segments, demonstrating the applicability of LAADF-STEM for extracting quantitative information from polymer systems.

EXPERIMENTAL SECTION

Sample Preparation. A criterion to choose the candidate polymers for LAADF-STEM analysis is that they should contain only light elements such as C, O, and H, so that it is basically very hard to produce sufficient contrast without proper staining in conventional TEM. In this study, two block copolymer systems were examined for their self-assembly or phase separation behavior by LAADF-STEM without any artificial precontrast-enhancements. The first copolymer is a diblock copolymer of poly(8-vinyloxytricyclo[5.2.1.0]decane vinyl ether)-*block*-poly(*n*-butyl vinyl ether), abbreviated poly(TCDVE)-*b*-poly(NBVE), which was synthesized as already reported (Figure S2a).[27] The poly(TCDVE)-*b*-poly(NBVE) with a molar ratio of *m*(TCDVE):*n*(NBVE) = 3:7 for the two segments was synthesized using living cationic polymerization, where the averaged molecular weight = 71 100 and M_w/M_n = 1.35. A similar triblock copolymer poly(TCDVE)-*b*-poly(NBVE)-*b*-poly(TCDVE) has been concluded to show granular microphase separation, from an atomic force microscopy (AFM) study,[27] and hence the poly(TCDVE)-*b*-poly(NBVE) is an appropriate sample to visualize any phase separation. This copolymer in a $CHCl_3$ solution (2.5 mg mL^{-1}) was spin-coated with 1500 rpm for 10 s on a cleaved (100) surface of a KCl single crystal, which served for AFM observations to examine the phase separation. The averaged film thickness was about 20−30 nm with a local roughness of about 2 nm as estimated by AFM. For STEM observations, the copolymer film on the KCl was floated off on a water surface and fixed on a microgrid. The second diblock copolymer is poly(vinylphenol)-*block*-polystyrene, abbreviated PVPh-*b*-PS, which was prepared by sequential living anion polymerization and subsequent hydrolytic deprotection as reported previously (Figure S2b).[28] This copolymer shows a clear-cut phase separation of lamellar type. For STEM observations, ultrathin sections of the sample were prepared using a Lica Ultracut S microtome with a diamond knife. Slices of about 50 nm thickness were cut at room temperature and fixed on a microgrid.

Atomic Force Microscopy. The phase separation of different segments in the copolymers was examined with atomic force microscopy (AFM; Digital Instruments, NanoScope IIIa). In order to observe the hard and soft domains, dynamic force microscopy was adopted for the spin-coated copolymer films on a single crystalline KCl {001} surface. The film surface was examined by phase imaging in addition to height imaging in a tapping mode, which was operated with a Si cantilever (Nanoworld PointProbe NCH).

Electron Microscopy. STEM observations were performed with a JEOL JEM-2200FS instrument operated at 200 kV. Mainly LAADF-STEM was adopted for observing the phase separations of poly(TCDVE)-*b*-poly(NBVE) and PVPh-*b*-PS without any artificial staining, which was expected to give image contrast depending on the mass thickness. The convergent angle was 12.3 mrad, and the detection angle was 20−53 mrad which corresponds to the range of the LAADF condition. This condition is highly suitable for producing contrast, as shown in Figures 1 and S3 for radiation-sensitive samples such as a thin crystalline polymer film and a typical phase separated triblock copolymer, respectively. The electron scattering profiles of a carbon atom are illustrated in Figure S4. Above 50 mrad of scattering angle (HAADF-STEM), the TDS is the dominant intensity, simply indicating quantitative incoherent imaging. In turn, below 50 mrad (LAADF-STEM), the TDS intensity becomes stronger, which means that the LAADF-STEM is more suitable to observe radiation-sensitive samples since the more TDS electrons can be available for imaging under the same intensity of incident electrons. However, since the elastic scattering is comparable in intensity to TDS in the LAADF-STEM condition, one should take the precaution of analyzing images quantitatively, and in particular, when there are crystalline diffractions in the LAADF range. The temperature dependence of the LAADF-STEM image intensity around glass-transitions of poly(TCDVE)-*b*-poly(NBVE) and PVPh-*b*-PS was examined using a cooling-holder (double tilt cryo-holder, Gatan, Inc.) and a heating holder (high temperature holder, JEOL) in the temperature ranges of −80 to +20 °C and 20−140 °C, respectively.

dx.doi.org/10.1021/ma4014934 | *Macromolecules* 2013, 46, 8589−8595

RESULTS AND DISCUSSION

Comparison of LAADF-STEM with HAADF-STEM Images. Before discussing the morphology of copolymers, it is useful and important to consider the effects of the detection angular ranges on ADF-STEM imaging. The signal-to-noise ratio (S/N) in the images was compared as a function of the detection angle (Figure S5). By investigating the images acquired with various detection angles, we experimentally verified that the S/N was lower for the HAADF condition, while a higher S/N was obtained for the LAADF condition as shown clearly in Figure S6. This indicates that the LAADF-STEM at a range lower than 50 mrad utilizes more TDS electrons than the HAADF condition above 50 mrad, as illustrated in Figure S4. In particular, such a strong scattering intensity becomes advantageous for observations of radiation-sensitive organic materials as reported for high-resolution molecular imaging.[23,24] It is worth noting that the polymer materials used in the present study are amorphous and are expected to show neither Bragg diffractions nor strong elastic scattering intensities, leading to substantive quantitative incoherent images even at LAADF-STEM detection angular ranges.

LAADF-STEM Image of poly(TCDVE)-*b*-poly(NBVE). The observed LAADF-STEM image of the diblock copolymer of poly(TCDVE)-*b*-poly(NBVE) shows a microphase-separated morphology of network structure at room temperature (Figure 2b). The images were obtained from particularly thin regions in the sample (Figure 2a). The bright contrast showing a network of ropes with a width of about 20 nm was assigned to the higher density parts of the glassy poly(TCDVE) with ρ(TCDVE) = 1.11 g cm^{-3} for the poly(TCDVE) homopolymer measured by an AccuPyc 1330 pycnometer, whereas the poly(NBVE) segments show dark contrast due to the rubbery phase with lower density of ρ(NBVE) = 0.95 g cm^{-3} for the corresponding homopolymer. This identification can also be rationalized from the compositional ratio between the poly(TCDVE) and poly(NBVE) segments, namely the higher density poly(TCDVE) is the minor component in the present case as m(TCDVE):n(NBVE) = 3:7. Since it is possible to synthesize copolymers with various values of the m:n ratio,[27] LAADF-STEM observations were carried out for a copolymer with the reverse ratio of m(TCDVE):n(NBVE) = 7:3. In this case, the brighter regions of the poly(TCDVE) segment occupy wider areas of the image (Figure S7), correlating well with the major component of the higher density poly(TCDVE) in the copolymer. The observed morphology is a disordered network of hard poly(TCDVE) segments with a short correlation length (persistent length) of less than 100 nm. Such a distorted morphology of intertwined network was observed in a diblock-coplymer of polystylene and poly(methyl methacrylate) (PMMA).[29] When annealed thermally applying an electric field, well-aligned cylinders of PMMA were formed near the electrodes. By annealing without such an applied field, however, the observed morphology was highly distorted as the present case.

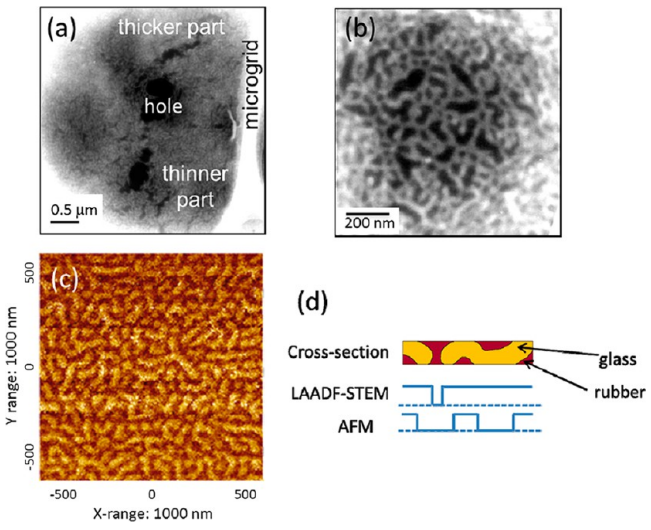

Figure 2. Comparison of images by LAADF-STEM and AFM of poly(TCDVE)-*b*-poly(NBVE). (a) Low-magnified and (b) high-magnified LAADF-STEM images of poly(TCDVE)-*b*-poly(NBVE), where the poly(TCDVE) segment is observed as a bright rod-like network with a width of 20 nm. (c) AFM dynamic phase image of poly(TCDVE)-*b*-poly(NBVE) spin-coated on the KCl {001} surface showing similar rod-like widths even though it is slightly shorter in length. (d) Schematics of the imaging mechanism in LAADF-STEM and AFM; AFM is sensitive to the surface and LAADF-STEM to the bulk.

The above assignment was also verified directly from complementary AFM observations. Figure 2c shows the typical AFM phase image with a tapping mode at room temperature. Similar to the LAADF-STEM image in Figure 2b, the network of ropes with about 20 nm-width was observed, where the brighter regions are related to the hard surfaces which should be the glassy poly(TCDVE) segments. There is, however, a slight discrepancy in the appearances of the LAADF-STEM and AFM images. The LAADF-STEM image shows the network of longer ropes compared to that of AFM. This could have originated from the difference in their imaging mechanism as explained schematically in the cross-sectional view of the film in Figure 2d. The transmitted LAADF-STEM images are bulk-sensitive, while the AFM images are surface-sensitive, resulting in the difference in the apparent length of the ropes. In AFM, the ropes with bright contrast seem to be cut into short pieces, while the morphology was revealed with longer and continuous ropes in LAADF-STEM. Since LAADF-STEM and AFM are complementary tools, we note that the LAADF-STEM by taking advantage of the bulk-sensitivity is an applicable method for quantitative observations of the 3D fine structures in copolymer films.

Contrast Change of LAADF-STEM Images Associated with T_g in Poly(TCDVE)-*b*-poly(NBVE). The T_g of poly(TCDVE) homopolymer was estimated to be about 100 °C,[30] and that of poly(NBVE) homopolymer was about −55 °C.[31] Thermal differential scanning calorimetry (DSC) analysis indicated that in the copolymer of m(TCDVE):n(NBVE) = 3:7, the two glass transition temperatures for the poly(NBVE) and poly(TCDVE) segments are around T_{g1} = −44 °C and T_{g2} = 73 °C, respectively (Figure S8). These temperatures are slightly different from the values of the corresponding homopolymers, possibly due to microphase formation. Then, the poly(NBVE) segment phase-transfers from the rubbery to glassy state around −44 °C upon cooling. Since the LAADF-STEM intensity is related quantitatively to the mass thickness at a local sample area, the glass transition possibly affects the change in the LAADF-STEM intensity as a function of temperature.

During the investigation of correlation between the LAADF-STEM intensity and glass transition, the intensity fluctuation of

dx.doi.org/10.1021/ma4014934 | Macromolecules 2013, 46, 8589−8595

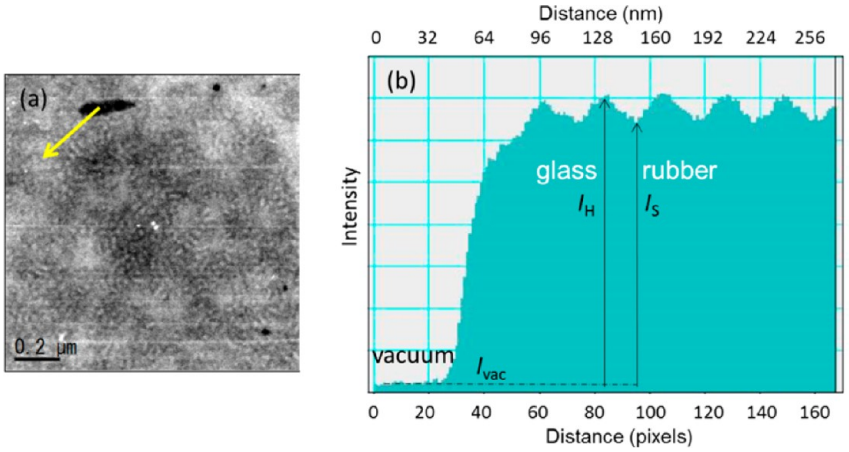

Figure 3. (a) LAADF-STEM image including a hole in the copolymer film. (b) Intensity profile measured along the yellow arrow in part a. I_H and I_S are the intensities of the brighter poly(TCDVE) part and the darker poly(NBVE) matrix part, respectively, and I_{vac} is the intensity in the vacuum region. To normalize the fluctuation of the incident electron beam during observations and local thickness variation, the image contrast C is defined as $C = (I_H - I_S)/I_H$.

the incident electron beam with time might hide real variations in relevant image intensities in the present experiments over a long period of time. Therefore, normalization of the measured intensities is indispensable for quantitative experiments with temperature change. In addition, since the thickness of the samples is directly proportional to STEM intensity, we should measure not the temperature changes of the intensity itself but rather changes in the following normalized local image contrast. We defined the local image contrast C as $C = (I_H - I_S)/I_H$, where I_H and I_S are the intensities of the hard and soft parts measured from the intensity obtained in the vacuum region, I_{vac}, in the LAADF-STEM images at each temperature as illustrated in Figure 3.

The polymers are often damaged easily by electron irradiation due to radical formation, chain session, and cross-linking, leading to serious damage including loss of crystallinity, mass-loss, morphology deformation, and contamination, which are the basic processes for both of TEM and STEM.[32] When the observation is performed by changing the specimen temperature, in order to minimize damage, it is essential either (i) to observe a different area on the specimen at each temperature or (ii) to carry out a few limited observations on the same area. As described before, LAADF-STEM is a more effective method to minimize such radiation damage by employing more TDS electrons. In the present study, we adopted the second procedure to obtain quantitative LAADF-STEM intensities at the same area, so as to reduce possible uncertainty from any substantial thickness differences. As discussed, the image contrast C is essential to compare changes in LAADF-STEM, but it was found experimentally that C is not sufficient to completely normalize intensities for too large different thicknesses possibly owing to inelastic scattering. In order to minimize experimental error, the LAADF-STEM observations were carried out at the same area during the slow cooling and heating processes. Therefore, the LAADF-STEM measurements in this study were limited to only several selected temperatures to avoid superfluous radiation damage as much as possible.

Figure 4 shows typical changes in LAADF-STEM images with changing temperature of poly(TCDVE)-*b*-poly(NBVE) at (a) 25 and (b) −63 °C, and again at (c) 25 °C after cooling down once below −70 °C. The images look very similar at the

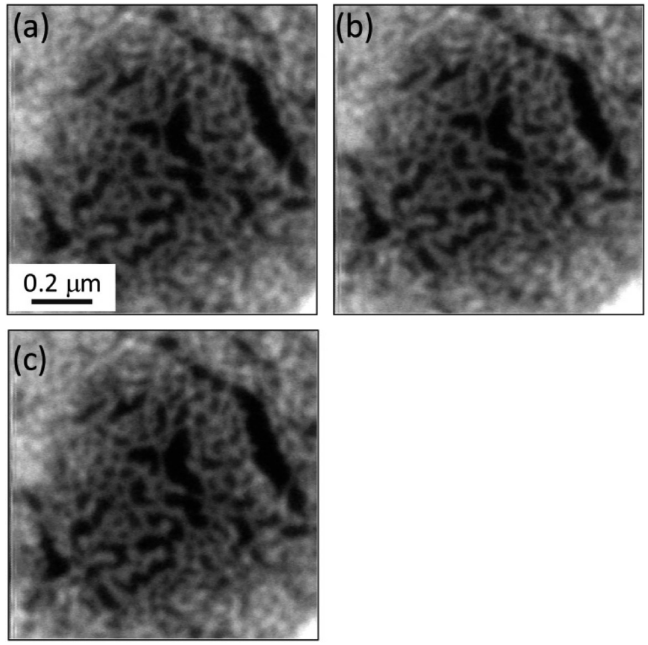

Figure 4. LAADF-STEM images of poly(TCDVE)-*b*-poly(NBVE) observed at (a) 25, (b) −63, and (c) 25 °C again after cooling below −70 °C. In parts a and c, the poly(NBVE) segment is rubbery and the poly(TCDVE) is glassy, while in part b, both segments are glassy. There is almost no specific change in morphology of the phase separation during the temperature change.

same specimen position without any large structural deformations. Under these experimental conditions, we can trace the temperature change of contrast without any serious radiation damages. Figure 5 shows the image contrast C extracted from the LAADF-STEM images as a function of temperature. This graph clearly shows that the contrast C has a distinct kink around −50 °C near the T_g of the poly(NBVE) segment, attributable to a big change in the temperature coefficient of thermal expansion due to the glass transition of the poly(NBVE) segment. Below −50 °C, the thermal expansion coefficients of both the poly(NBVE) and poly(TCDVE) segments with the glassy phases could be regarded as small and almost the same, resulting in a nearly flat

dx.doi.org/10.1021/ma4014934 | *Macromolecules* 2013, 46, 8589−8595

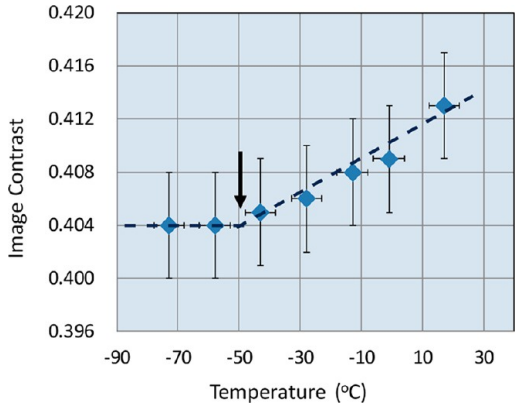

Figure 5. LAADF-STEM image contrast C of poly(TCDVE)-*b*-poly(NBVE) measured between −80 and +25 °C. A kink in the plot was observed around −50 °C, which corresponds to the T_g of the poly(NBVE) phase.

temperature dependence of the contrast C. On the other hand, above −50 °C where the volume of the rubbery poly(NBVE) phase expands more against that of the glassy poly(TCDVE) phase, the slope corresponds to the difference in the density change of the rubbery poly(NBVE) and the glassy poly(TCDVE), when assuming an almost constant I_H within the temperature range. This is resulted from stronger 3D shrinkage of the soft segments upon cooling, inducing the increase in the STEM intensity of the rubbery poly(NBVE) and then the decrease in contrast C as explained schematically in Figure S9. The difference in the thermal expansion coefficients can be estimated from Figure 5 as $\alpha_{rubber} - \alpha_{glass} = \Delta\alpha = 1 \times 10^{-4}$ K^{-1}, which could be slightly small as the difference in the rubbery and glassy states. It is worthwhile noting that the LAADF-STEM images somewhat overlap with the glassy and rubbery segments projected along the incident beam direction, so that the image intensity might not correlate simply to the difference in density for the two phases.

T_g is known to depend on the domain size or the thickness of the films when formed on substrates. In the case of a 10 nm-thick PS film on a Si substrate, T_g was reported to decrease about 10 °C from that of the bulk,[33] and T_g of PMMA on a gold surface was reported to decrease with decreasing film thickness, in accordance with the result for PS. In contrast, T_g increases slightly on a native oxide of silicon with decreasing thickness, because the hydrogen bonding at the interface restricts mobility and leads to an increase in T_g.[34] The present thin film has a thickness of around 10−20 nm, so that some change in T_g with respect to the bulk might be expected. But in the present case, there is almost no difference in T_g between the thin film and the bulk, within experimental error, meaning either the size (thickness) might be sufficiently big already for the copolymer or no surface effects are anticipated because of the free-standing film.

Contrast Change of LAADF-STEM Images Associated with T_g in PVPh-*b*-PS. As pointed out already, the LAADF-STEM images of poly(TCDVE)-*b*-poly(NBVE) are somewhat overlapped by the hard and soft segments and depend on how they mix in the film along the beam direction. Therefore, the image intensity might not correlate simply to the difference in density for the two phases. Accordingly, in order to estimate T_g more precisely by LAADF-STEM, it is desirable to choose another sample having more clear microphase-separated domains. A second copolymer of PVPh-*b*-PS was investigated to examine its T_g by LAADF-STEM, since it exhibits clear lamellar phase-separation as shown in Figure 6. The sharp

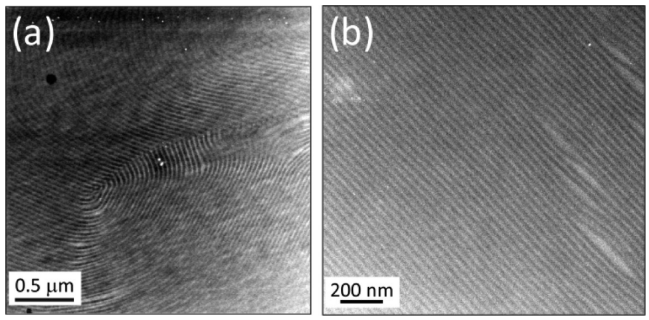

Figure 6. (a) Low- and (b) high-magnification LAADF-STEM images of PVPh-*b*-PS without any artificial staining. Both copolymer components are glassy at room temperature, and the contrast is produced by the difference in their density; ρ(PS) = 1.05 g cm^{-3} for the PS component and ρ(PVPh) = 1.20 g cm^{-3} for the PVPh component. The images show a microphase-separated lamellar structure with the brighter PVPh layers.

lamellae microphase separation allows us to measure directly the density difference between the two phases. In order to minimize experimental error, the LAADF-STEM observations were carried out again at the same sample area but at several different domains with well-ordered lamellae in the slow heating and cooling processes. The LAADF-STEM measurements were limited to several selected temperatures to avoid serious deformation by radiation damage as much as possible.

The PVPh and PS segments are both glassy states at room temperature. The PS homopolymer changes into a rubbery state around 100 °C, while the PVPh was reported to reveal a large scatter of T_g between 53 and 194 °C, which was attributed to residual moisture and/or solvent in the samples and also partially to the molecular weight.[35] Recently, the T_g of the PVPh homopolymer was determined to be about 175.0−179.5 °C for vacuum-dried samples.[35] Only the T_g of the PS component was expected to be detected by LAADF-STEM measurements in the temperature range between 20 and 150 °C. Figure 7 shows the temperature change effect on the LAADF-STEM image contrast C of PVPh-*b*-PS. We found a clear kink around 90 °C which corresponds to the T_g of the PS segment, even though it is slightly lower than the usual T_g of

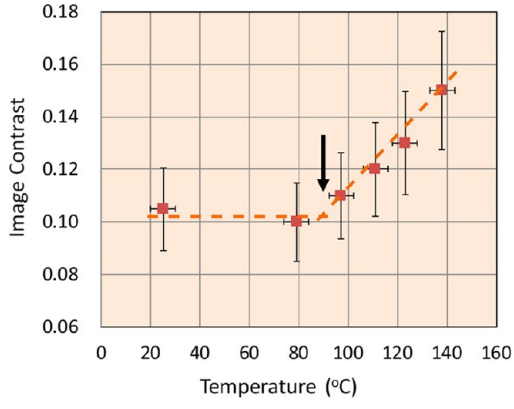

Figure 7. LAADF-STEM image contrast C of PVPh-*b*-PS measured between 20 and 150 °C. A kink in the plot was observed at around 90 °C, which corresponds well to the T_g of the PS phase.

dx.doi.org/10.1021/ma4014934 | *Macromolecules* 2013, 46, 8589−8595

the PS homopolymer. Here again, the T_g of the thin free-standing film seems not to change so much from that of the bulk state. Since the contrast C can be regarded as the density difference between the glassy and rubbery states, the slope above 90 °C in Figure 7 corresponds to the difference in the intensity change of the rubbery PS and the glassy PVPh, when assuming a constant I_H in the temperature range considered. The difference in the thermal expansion coefficients can then be estimated to be $\Delta\alpha = 7 \times 10^{-4}$ K^{-1} from the slope, which is larger than the case of poly(TCDVE)-*b*-poly(NBVE). The thermal expansion coefficients of PS are $\alpha_{glass} = 2 \times 10^{-4}$ K^{-1} and $\alpha_{rubber} = 7 \times 10^{-4}$ K^{-1},[33] and the expected difference $\Delta\alpha = 5 \times 10^{-4}$ K^{-1} agrees reasonably well with the present experimental results.

CONCLUSIONS

In this study, LAADF-STEM was applied to nanoscale analysis for the glass transition of two block copolymers with microphase separation. We verified that the LAADF-STEM imaging formed contrast of the fine structures in the block copolymers without any staining. The LAADF-STEM image of the poly(TCDVE)-*b*-poly(NBVE) showed a network of ropes attributable to the glassy poly(TCDVE) in rubbery poly(NBVE) matrix phases. On the other hand, the image of PVPh-*b*-PS showed lamellar phase separation structures of the hard PVPh and soft PS phases. Moreover, investigating the image contrast C as a function of temperature change allowed estimation of the glass transition temperature T_g of the components in the block copolymers. In a cooling experiment for the poly(TCDVE)-*b*-poly(NBVE), the contrast C indicated a distinct kink around −50 °C at the T_g of the poly(NBVE) segment. In turn, for the heating experiment for PVPh-*b*-PS, the contrast C showed a distinct kink around 90 °C at the T_g of the PS segment. These estimated T_g values agreed well with those acquired by DSC measurements. AFM is the well-known tool to examine surface glass transition temperatures,[36] and the present LAADF-STEM is in a complementary position in nanoscale T_g measurements because of its bulk sensitivity. In addition, the temperature dependence of C in LAADF-STEM allows us to quantitatively estimate the difference in thermal expansion coefficients of rubbery and glassy components. The results indicate that LAADF-STEM imaging has a high potential to form image contrast without any staining and is a promising tool to quantitatively analyze nanoscale phases of polymer materials.

ASSOCIATED CONTENT

Supporting Information

Schematic illustration of ADF-STEM and BF-STEM, examples of LAADF-STEM images, chemical structures of samples, comparison between TEM and LAADF-STEM images, scattering profiles in STEM, detection angle dependence of STEM contrast and S/N, and illustration of temperature change of films. This material is available free of charge via the Internet at http://pubs.acs.org.

AUTHOR INFORMATION

Corresponding Authors

*E-mail: (R.A.) aso@eels.kuicr.kyoto-u.ac.jp.
*E-mail: (S.I.) isoda@icems.kyoto-u.ac.jp.

Author Contributions

The manuscript was written through contributions by all authors. All authors have given approval to the final version of the manuscript.

Notes

The authors declare no competing financial interest.

ACKNOWLEDGMENTS

This work was partly supported by Grants-in-Aid for Scientific Research, Grants No. 20550188 and 23310075 from MEXT, Japan.

REFERENCES

(1) Dalton, L. *Adv. Polym. Sci.* **2002**, *158*, 1−86.
(2) Roncali, J.; Leriche, P.; Cravin, A. *Adv. Mater.* **2007**, *19*, 2045−2060.
(3) O'Neill, M.; Kelly, S. M. *Adv. Mater.* **2011**, *5*, 566−584.
(4) Hayat, M. A. *Principles and techniques of electron microscopy: biological applications*; Cambridge University Press: Cambridge, U.K., 2000,
(5) Chesne, A. D.; Lieser, G.; Wegner, G. *Colloid Polym. Sci.* **1994**, *272*, 1329−1342.
(6) Yamauchi, K.; Takahashi, K.; Hasegawa, H.; Iatrou, H.; Hadjichristidis, N.; Kaneko, T.; Nishikawa, Y.; Jinnai, H.; Matsui, T.; Nishioka, H.; Shimizu, M.; Furukawa, H. *Macromolecules* **2003**, *36*, 6962−6966.
(7) Tosaka, M.; Danev, R.; Nagayama, K. *Macromolecules* **2005**, *38*, 7884−7886.
(8) Shiue, J.; Chang, C. S.; Huang, S. H.; Hsu, C. H.; Tsai, J. S.; Chang, W. H.; Wu, Y. M.; Lin, Y. C.; Kuo, P. C.; Huang, Y. S.; Hwu, Y. K.; Kai, J. J.; Tseng, F. G.; Chen, F. R. *J. Electron Micros.* **2009**, *58*, 137−145.
(9) Smith, R. W.; Bryg, V. *Rubber Chem. Technol.* **2006**, *79*, 520−540.
(10) Nellist, P. D.; Pennycook, S. J. *Ultramicroscopy* **1999**, *78*, 111−124.
(11) Nellist, P. D.; Pennycook, S. J. *Adv. Imaging Electron Phys.* **2000**, *113*, 147−203.
(12) Isoda, S. *Abstr. China-Neth. Bilat. Symp. Electron Micros. Polym. Syst.* **2007**, 9−11.
(13) Loos, J.; Sourty, E.; Lu, K.; With, G.; Bavel, S. *Macromolecules* **2009**, *42*, 2581−2586.
(14) Sourty, E.; Bavel, S.; Lu, K.; Guerra, R.; Bar, G.; Loos, J. *Microsc. Microanal.* **2009**, *15*, 251−258.
(15) Kaneko, T.; Motoki, S.; Aoyama, Y.; Nichioka, H.; Ohkura, Y.; Kondo, Y.; Jinnai, H. *Microsc. Microanal.* **2009**, *15* (Suppl 2), 630−631.
(16) Lu, K.; Sourty, E.; Loos, J. *J. Electron Microsc.* **2010**, *59*, S39−S44.
(17) Hollinger, J.; Jahnke, A. A.; Coombs, N.; Seferos, D. S. *J. Am. Chem. Soc.* **2010**, *132*, 8546−8547.
(18) Li, S. S.; Chang, C. P.; Lin, C. C.; Lin, Y. Y.; Chang, C. H.; Yang, J. R.; Chu, M. W.; Chen, C. W. *J. Am. Chem. Soc.* **2011**, *133*, 11614−11620.
(19) Klein, M. F. G.; Pfaff, M.; Müller, E.; Czolk, J.; Reinhard, M.; Valouch, S.; Lemmer, U.; Colsmann, A.; Gerthsen, D. *J. Polym. Sci., Part B Polym. Phys.* **2012**, *50*, 198−206.
(20) Treat, N. D.; Varotto, A.; Takacs, C. J.; Batara, N.; Al-Hashimi, M.; Heeney, M. J.; Heeger, A. J.; Wudl, F.; Hawker, C. J.; Chabinyc, M. L. *J. Am. Chem. Soc.* **2012**, *134*, 15869−15879.
(21) Choi, S. H.; Liman, C. D.; Krämer, S.; Chabinyc, M. L.; Kramer, E. J. *J Phys. Chem. B* **2012**, *116*, 13568−13574.
(22) Schaper, A. K.; Kurata, H.; Yoshioka, T.; Tsuji, M. *Microsc. Microanal.* **2007**, *13*, 336−341.
(23) Haruta, M.; Yoshida, K.; Kurata, H.; Isoda, S. *Ultramicroscopy* **2008**, *108*, 545−551.
(24) Haruta, M.; Kurata, H.; Isoda, S. *Fullerene, Nanotubes Carbon Nanostruct.* **2008**, *16*, 454−462.

(25) Yu, Z.; Muller, D. A.; Silcox, J. *J. Appl. Phys.* **2004**, *95*, 3362−3371.
(26) Egerton, R. F. *Ultramicroscopy* **2013**, *127*, 100−108.
(27) Hashimoto, T.; Namikoshi, T.; Irie, S.; Urushisaki, M.; Sakaguchi, T.; Nemoto, T.; Isoda, S. *J. Polymer Sci. Part A, Polymer Chem.* **2008**, *46*, 1902−1906.
(28) Tung, P. H.; Kuo, S. W.; Chan, S. C.; Hsu, C. H.; Wang, C. F.; Chang, F. C. *Macromol. Chem. Phys.* **2007**, *208*, 1823−1831.
(29) Morkved, T. L.; Lu, M.; Urbas, A. M.; Ehrichs, E. E.; Jaeger, H. M.; Mansky, P.; Russell, T. P. *Science* **1996**, *273*, 931−933.
(30) Namikoshi, T.; Hashimoto, T.; Kodaira, T. *J. Polym. Sci., Part A: Polym. Chem.* **2004**, *42*, 3649−3653.
(31) Namikoshi, T.; Hashimoto, T.; Urushisaki, M. *J. Polym. Sci., Part A: Polym. Chem.* **2007**, *45*, 4855−4866.
(32) Reimer, L. *Transmission Electron Microscopy*; Springer-Verlag: Berlin, 1984.
(33) Keddie, J. L.; Jones, R. A. L.; Cory, R. A. *Europhys. Lett.* **1994**, *27*, 59−64.
(34) Keddie, J. L.; Jones, R. A. L.; Cory, R. A. *Faraday Discuss.* **1994**, *98*, 219−230.
(35) Kratochvíl, J.; Šturcová, A.; Sikora, A.; Dybal, J. *Eur. Polym. J.* **2009**, *45*, 1851−1856.
(36) Overney, R. M.; Buenviaje, C.; Luginbühl, R.; Dinelli, F. *J. Therm. Anal. Calorim.* **2000**, *59*, 205−225.